

# **Analysis of multiple cracking in metal/ceramic composites with lamellar microstructure**

M. Kashtalyan<sup>1</sup>, Y. Sinchuk<sup>2</sup>, R.Piat<sup>2,3</sup>, I. Guz\*<sup>1</sup>

<sup>1</sup>Centre for Micro- and Nanomechanics (CEMINACS), School of Engineering, University of Aberdeen, Fraser Noble Building, Aberdeen AB24 3UE, UK

<sup>2</sup> Institute of Engineering Mechanics, Karlsruhe Institute of Technology, Kaiserstrasse 12, 76131 Karlsruhe, Germany

<sup>3</sup> Faculty of Mathematics and Natural Sciences, University of Applied Sciences Darmstadt, Haardtring 100, 64295 Darmstadt, Germany

\*Corresponding author: i.guz@abdn.ac.uk, tel.: +44 (0)1224 272808, fax.: +44 (0)1224 272808

## **KEYWORDS**

Metal/ceramic composites; Transverse cracking; Damage modelling; Finite Element Modeling; Analytical modeling

## **ABSTRACT**

Metal/ceramic composites with lamellar microstructures are a novel class of metal-matrix composites produced by infiltration of freeze-cast or ice-templated ceramic preforms with molten aluminium alloy. The cost-effectiveness of production and relatively high ceramic content make such composites attractive to a number of potential applications in the automotive, aerospace and biomedical engineering. A hierarchical lamellar microstructure exhibited by these composites, with randomly orientated domains in which all ceramic and metallic lamellae are parallel to each other, is the result of the ice crystal formation during

freeze-casting or ice templating of preforms from water-ceramic suspensions. In this paper, a single-domain sample of metal/ceramic composite with lamellar microstructure is modeled theoretically using a combination of analytical and computational means. Stress field in the sample containing multiple transverse cracks in the ceramic layer is determined using a modified 2-D shear lag approach and a finite element method. Using finite element modeling the shear layer thickness is determined and used as input in the analytical model. Degradation of stiffness properties of the sample due to multiple transverse cracking is predicted using the Equivalent Constraint Model.

#### ACKNOWLEDGMENTS AND FUNDING INFORMATION

Financial support of this research by The Royal Society, UK (IE121116), The Carnegie Trust for the Universities of Scotland, UK (Trust Reference 31747) and DFG (PI 785/3-2, PI 785/1-2), Germany, is gratefully acknowledged. We thank Dr. S. Roy (KIT) for providing the microstructure images and Professor I. Tsukrov (University of New Hampshire, USA) for helpful discussions.

## 1. INTRODUCTION

Metal-matrix composites are material systems in which metal is combined with another, often non-metallic, material to produce a novel material with superior engineering properties. Metal-matrix composites offer many advantages over monolithic metals and their alloys such as high specific stiffness and strength, better creep, fatigue and wear resistance, and good thermal properties (Clyne, 2000; Evans A, San Marchi and Mortensen, 2003; Miracle, 2005; Chawla and Chawla 2006).

In the recent decades, significant advances have been made in the field leading to increase in the number of reinforcements as well as processing routes available (Mortensen and Llorca, 2010). One of the new classes of metal-matrix composites that have emerged during this time are interpenetrating phase composites, in which ceramic preforms with open porosity are infiltrated with molten metal or alloy to produce composites with two three-dimensionally interpenetrating constituents (Mortensen and Llorca 2010). Metal/ceramic interpenetrating phase composites possess production dependent ceramic content and exhibit highly sophisticated internal microstructures that depend on the preform fabrication method.

Several innovative methods have been developed to produce open-pore ceramic preforms (Mortensen and Llorca, 2010). One of them – freeze casting – is based on the physics of ice formation and involves controlled directional freezing of concentrated water-ceramic suspension (Fukasawa et al, 2002; Mattern et al, 2004; Deville et al, 2006). Growing ice crystals push fine ceramic particles forcing them to form thin parallel and connected layers, creating a lamellar microstructure. The ice is subsequently sublimated by freeze drying. The resulting ceramic preforms exhibit pronounced open porosity and mechanical strength and can be infiltrated with either organic or inorganic phase.

Wanner and Roy (2008) have studied metal-ceramic composites produced at Institute of Applied Materials-Ceramic Materials and Technologies at Karlsruhe Institute of Technology, Karlsruhe, Germany. These composites were produced from alumina preforms prepared by freeze-casting and subsequent sintering by infiltrating them with aluminium-silicon alloy using a squeeze-casting technique. The resulting metal/ceramic composites were found to possess hierarchical lamellar microstructure with randomly orientated individual regions (domains), in which all ceramic and metallic lamellae are parallel to each other. Domains had sizes of up to several millimeters while thicknesses of alternating ceramics and metallic lamellae were from 20 to 200  $\mu\text{m}$  (Roy and Wanner 2008). Individual domains were found to exhibit a pronounced anisotropy, with the freezing direction being the stiffest and strongest. Failure in this direction occurred in a brittle manner, while other directions were controlled by the alloy and exhibited extensive ductility (Roy, Butz and Wanner, 2010). In the subsequent studies, complete set of anisotropic elastic properties of these composites was determined experimentally using ultrasound phase spectroscopy and resonant ultrasound spectroscopy and predicted using micromechanical modelling (Ziegler et al, 2010, Roy et al, 2011). A study of single-domain samples taken from these composites was also undertaken (Sinchuk et al, 2013) focusing on the compressive response and elasto-plastic behavior. Launey et al (2010) used freeze-casting or 'ice templating' to create fine scale laminated metal/ceramic bulk composites, with ceramic contents of 36% and with lamellae thickness down to 10 microns, fracture toughness of  $40 \text{ MPa}\cdot\text{m}^{0.5}$  and tensile strength of approximately 300 MPa.

Damage mechanisms in metal/ceramic composites with lamellar microstructures have not been studied in depth yet. Previous studies of cracking patterns in metal/ceramic composites under tensile loading were performed on composites fabricated by diffusion bonding and focused mainly on multiple cracking in ceramic layers ahead of a macroscopic through crack

(Huang and Zhang 1994, 1996; Shaw et al, 1996; Hwu and Derby, 1999a,b). Initiation and accumulation of damage within the ceramic lamellae, mainly in the form of transverse cracking, Fig. 1, has been observed under compressive loading. It is also expected to occur under tensile loading due to failure strain of ceramics being less than that of the metal.

In this paper, a single-domain sample of metal/ceramic composite with lamellar microstructure is modeled theoretically using a combination of analytical and computational means. Stress field in the sample containing multiple transverse cracks in the ceramic layer is determined using a modified 2-D shear lag approach (Kashtalyan and Soutis, 2011; Katerelos et al, 2008) and a finite element method. The Equivalent Constraint Model is then applied to predict degradation of stiffness properties of the sample due to multiple transverse cracking.

## 2. ANALYTICAL MODELLING

### 2.1 STRESS ANALYSIS

Consider a metal/ceramic composite sample consisting of a ceramic layer of thickness  $2h_c$  fully bonded between two metal layers of thickness  $h_m$ . Ceramic layer contains multiple tunneling cracks, assumed to be spaced uniformly with crack spacing  $S = 2s$ , spanning the full thickness of the ceramic layer and depth  $2w$  of the sample. The sample is referred to the co-ordinate system  $x_1x_2x_3$ , with  $x_1$  axis parallel to the cracks (Fig. 2) and subjected to biaxial tension  $\bar{\sigma}_{11}$ ,  $\bar{\sigma}_{22}$  and in-plane shear loading  $\bar{\sigma}_{12}$ . Due to periodicity of damage and symmetry of the sample, only a quarter of the representative segment bounded by two cracks needs to be considered (Fig. 2). The equilibrium equations in terms of microstresses, i.e. stresses averaged across the thickness of the layer and the depth of the sample, have the form

$$\chi \tilde{\sigma}_{ij}^{(m)} + \tilde{\sigma}_{ij}^{(c)} = (1 + \chi) \bar{\sigma}_{ij}, \quad i, j = 1, 2, \quad \chi = h_m / h_c \quad (1a)$$

$$\frac{d\tilde{\sigma}_{22}^{(c)}}{dx_2} + \frac{\tau_2}{h_c} = 0, \quad \frac{d\tilde{\sigma}_{12}^{(c)}}{dx_2} + \frac{\tau_1}{h_c} = 0, \quad (1b)$$

$$\tilde{\sigma}_{ij}^{(c)} = \frac{1}{2wh_c} \int_{-w-h_c}^w \int_{-h_c}^{h_c} \sigma_{ij}^{(c)}(x_1, x_2, x_3) dx_1 dx_3 \quad (1c)$$

where  $\tau_1, \tau_2$  are the interface shear stresses at the metal/ceramics interface. Assuming that out-of-plane shear stresses vary linearly with  $x_3$  and in the metal layer this variation is restricted to the shear layer of thickness  $h_s$  (Fig. 3), so that

$$\begin{aligned} \sigma_{j3}^{(c)} &= \frac{\tau_j}{h_c} x_3, \quad |x_3| < h_c; \\ \sigma_{j3}^{(m)} &= \frac{\tau_j}{h_s} (h_c + h_s - x_3), \quad h_c < |x_3| < h_c + h_s, \quad j = 1, 2 \end{aligned} \quad (2)$$

the interface shear stresses  $\tau_1, \tau_2$  can be expressed in terms of the in-plane displacements

$\tilde{u}_j^{(c)}, \tilde{u}_j^{(m)}, j = 1, 2$ , and shear moduli  $G_c, G_m$  of ceramic and metal as

$$\begin{aligned} \tau_j &= K_j (\tilde{u}_j^{(m)} - \tilde{u}_j^{(c)}), \\ K_j &= \frac{3G_c G_m}{h_c G_m + (1 + (1 - \eta)/2)\eta h_m G_c}, \quad \eta = h_s / h_m. \end{aligned} \quad (3)$$

The constitutive equations in terms of microstrains and microstresses are

$$\begin{bmatrix} \tilde{\epsilon}_{11}^{(c)} \\ \tilde{\epsilon}_{22}^{(c)} \\ \tilde{\gamma}_{12}^{(c)} \end{bmatrix} = \begin{bmatrix} S_{11}^{(c)} & S_{12}^{(c)} & 0 \\ S_{12}^{(c)} & S_{22}^{(c)} & 0 \\ 0 & 0 & S_{66}^{(c)} \end{bmatrix} \begin{bmatrix} \tilde{\sigma}_{11}^{(c)} \\ \tilde{\sigma}_{22}^{(c)} \\ \tilde{\sigma}_{12}^{(c)} \end{bmatrix}, \quad \begin{bmatrix} \tilde{\epsilon}_{11}^{(m)} \\ \tilde{\epsilon}_{22}^{(m)} \\ \tilde{\gamma}_{12}^{(m)} \end{bmatrix} = \begin{bmatrix} S_{11}^{(m)} & S_{12}^{(m)} & 0 \\ S_{12}^{(m)} & S_{22}^{(m)} & 0 \\ 0 & 0 & S_{66}^{(m)} \end{bmatrix} \begin{bmatrix} \tilde{\sigma}_{11}^{(m)} \\ \tilde{\sigma}_{22}^{(m)} \\ \tilde{\sigma}_{12}^{(m)} \end{bmatrix} \quad (4)$$

In addition, it is also assumed that  $\tilde{\varepsilon}_{11}^{(c)} = \tilde{\varepsilon}_{11}^{(m)}$ , and crack surfaces are stress-free, i.e.

$$\tilde{\sigma}_{22}^{(c)} \Big|_{x_2=\pm s} = 0, \quad \tilde{\sigma}_{12}^{(c)} \Big|_{x_2=\pm s} = 0 \quad (5)$$

Equations (1)-(4) can be reduced to two uncoupled second-order ordinary differential equations with respect to in-plane microstresses in the ceramic layer

$$\frac{d^2 \tilde{\sigma}_{22}^{(c)}}{dx_2^2} - L_1^{(c)} \tilde{\sigma}_{22}^{(c)} + \Omega_{11}^{(c)} \bar{\sigma}_{11} + \Omega_{22}^{(c)} \bar{\sigma}_{22} = 0, \quad \frac{d^2 \tilde{\sigma}_{12}^{(c)}}{dx_2^2} - L_2^{(c)} \tilde{\sigma}_{12}^{(c)} + \Omega_{12}^{(c)} \bar{\sigma}_{12} = 0 \quad (6)$$

Solutions of these equations satisfying specified boundary conditions can be found as

$$\begin{aligned} \tilde{\sigma}_{22}^{(c)} &= \frac{1}{L_1^{(c)}} \left( 1 - \frac{\cosh \sqrt{L_1^{(c)}} x_2}{\cosh \sqrt{L_1^{(c)}} s} \right) (\Omega_{11}^{(c)} \bar{\sigma}_{11} + \Omega_{22}^{(c)} \bar{\sigma}_{22}), \\ \tilde{\sigma}_{12}^{(c)} &= \frac{1}{L_2^{(c)}} \left( 1 - \frac{\cosh \sqrt{L_2^{(c)}} x_2}{\cosh \sqrt{L_2^{(c)}} s} \right) \Omega_{12}^{(c)} \bar{\sigma}_{12} \end{aligned} \quad (7a)$$

$$\begin{aligned} L_1^{(c)} &= \frac{K_2}{h_m} [S_{22}^{(m)} + \chi S_{22}^{(c)} + a_1 (S_{12}^{(m)} + \chi S_{12}^{(c)})], \\ L_2^{(c)} &= \frac{K_1}{h_m} (S_{66}^{(m)} + \chi S_{66}^{(c)}), \\ \Omega_{11}^{(c)} &= \frac{K_2}{h_m} (1 + \chi) (S_{12}^{(m)} + a_1 S_{11}^{(m)}), \\ \Omega_{22}^{(c)} &= \frac{K_2}{h_m} (1 + \chi) (S_{22}^{(m)} + a_1 S_{12}^{(m)}), \\ \Omega_{12}^{(c)} &= \frac{K_1}{h_m} (1 + \chi) S_{66}^{(m)}, \\ a_1 &= - \frac{S_{12}^{(m)} + \chi S_{12}^{(c)}}{S_{11}^{(m)} + \chi S_{11}^{(c)}} \end{aligned} \quad (7b)$$

The in-plane microstresses in the ceramic layer containing multiple transverse cracks can be used to evaluate the reduction of stiffness properties of the metal/ceramic composite single domain sample due to damage.

## 2.2 STIFFNESS REDUCTION

Let us consider an equivalent constraint laminate, in which the damaged layer is replaced with an equivalent homogeneous layer with degraded stiffness properties. The constitutive equations of the ‘equivalent’ layer in the co-ordinate system  $x_1, x_2, x_3$  (Fig. 2) are

$$\{\bar{\sigma}^{(c)}\} = [\bar{Q}^{(c)}] \{\bar{\varepsilon}^{(c)}\} \quad (8)$$

The reduced in-plane stiffness matrix  $[\bar{Q}^{(c)}]$  of this equivalent homogeneous layer is related to the in-plane stiffness matrix  $[\hat{Q}^{(c)}]$  of the undamaged ceramic layer via the In-situ Damage Effective Functions (IDEFs)  $\Lambda_{22}^{(c)}, \Lambda_{66}^{(c)}$  (Zhang, Fan and Soutis, 1992; Kashtalyan and Soutis, 1999, 2006, 2013) as

$$[\bar{Q}^{(c)}] = [\hat{Q}^{(c)}] - \begin{bmatrix} \frac{(\hat{Q}_{12}^{(c)})^2}{\hat{Q}_{22}^{(c)}} \Lambda_{22}^{(c)} & \hat{Q}_{12}^{(c)} \Lambda_{22}^{(c)} & 0 \\ \hat{Q}_{12}^{(c)} \Lambda_{22}^{(c)} & \hat{Q}_{22}^{(c)} \Lambda_{22}^{(c)} & 0 \\ 0 & 0 & \hat{Q}_{66}^{(2)} \Lambda_{66}^{(c)} \end{bmatrix} \quad (9)$$

The IDEFs  $\Lambda_{22}^{(c)}, \Lambda_{66}^{(c)}$  can be expressed in terms of macrostresses  $\bar{\sigma}_{ij}^{(c)}$  and macrostrains  $\bar{\varepsilon}_{ij}^{(c)}$  as



$$\Lambda_{22}^{(c)} = 1 - \frac{\bar{\sigma}_{22}^{(c)}}{\hat{Q}_{12}^{(c)} \bar{\varepsilon}_{11}^{(c)} + \hat{Q}_{22}^{(c)} \bar{\varepsilon}_{22}^{(c)}}, \quad \Lambda_{66}^{(c)} = 1 - \frac{\bar{\sigma}_{12}^{(c)}}{\hat{Q}_{66}^{(c)} \bar{\varepsilon}_{12}^{(c)}} \quad (10)$$

Once the in-plane microstresses  $\tilde{\sigma}_{ij}^{(2)}$  and microstrains  $\tilde{\varepsilon}_{ij}^{(2)}$  (i.e. stresses and strains averaged across the layer thickness and sample width) are known from the micromechanical analysis, the macrostresses and macrostrains can be found as

$$\bar{\sigma}_{ij}^{(c)} = \frac{1}{2s} \int_{-s}^s \tilde{\sigma}_{ij}^{(c)} dx_2, \quad \bar{\varepsilon}_{ij}^{(c)} = \bar{\varepsilon}_{ij}^{(m)} = \bar{\varepsilon}_{ij} = \frac{1}{2s} \int_{-s}^s \tilde{\varepsilon}_{ij}^{(c)} dx_2. \quad (11)$$

By substituting Eqn (6a) into Eqn (10) and then into Eqn (9), closed-form expressions for the IDEFs, representing them as explicit functions of the relative transverse crack density  $D_c = h_c / s$  are obtained

$$\Lambda_{22}^{(c)} = 1 - \frac{1 - \frac{D_c}{\lambda_1^{(c)}} \tanh\left[\frac{\lambda_1^{(c)}}{D_c}\right]}{1 + \alpha_1^{(c)} \frac{D_c}{\lambda_1^{(c)}} \tanh\left[\frac{\lambda_1^{(c)}}{D_c}\right]}, \quad \Lambda_{66}^{(c)} = 1 - \frac{1 - \frac{D_c}{\lambda_2^{(c)}} \tanh\left[\frac{\lambda_2^{(c)}}{D_c}\right]}{1 + \alpha_2^{(c)} \frac{D_c}{\lambda_2^{(c)}} \tanh\left[\frac{\lambda_2^{(c)}}{D_c}\right]} \quad (12)$$

Here the constants  $\lambda_i^{(c)} = h_c \sqrt{L_i^{(c)}}$  and  $\alpha_i^{(c)}$ ,  $i = 1, 2$ , depend solely on the compliances  $\hat{S}_{ij}^{(m)}$ ,  $\hat{S}_{ij}^{(c)}$  of metal and ceramic layer respectively, the shear lag parameters  $K_j$  and the layer thickness ratio  $\chi$ , whereas

$$\alpha_1^{(c)} = \frac{1}{\chi} [\hat{Q}_{22}^{(c)} (\hat{S}_{22}^{(m)} + a_1 \hat{S}_{12}^{(m)}) + \hat{Q}_{12}^{(c)} (\hat{S}_{12}^{(m)} + a_1 \hat{S}_{11}^{(m)})], \quad \alpha_2^{(c)} = \frac{1}{\chi} \hat{Q}_{66}^{(c)} \hat{S}_{66}^{(m)}. \quad (13)$$

### 3. NUMERICAL MODELLING

Analytical modelling was accompanied by numerical studies of the microstructure. The aims of these studies were to verify the results of the analytical modelling and also to estimate numerically the thickness of the shear layer  $h_s$  introduced in the analytical model. For this purpose the finite element (FE) modelling in ABAQUS (ABAQUS, 2015) was employed.

Firstly, FE model of a Plexiglas (PMMA) plate specimen containing a set of four parallel cracks was developed to enable comparison with experimental and numerical results of Bai and Pollard (2000); please refer to Fig.8 and Fig.1 in (Bai and Pollard, 2000) for a sketch of the experimental specimen and FE model, respectively. In the present study, only a quarter of the specimen was modelled in ABAQUS taking into account symmetry of the specimen. Meshed geometry used in the present study is shown in Fig. 4. The elastic properties of the Plexiglas (PMMA) were taken as follows: for the fractured ( $f$ ) and the neighbouring ( $n$ ) layers:  $E_n = E_f = 40 \text{ GPa}$ ,  $\nu_n = \nu_f = 0.2$ . Numerical results obtained in the current study give practically the same stress distribution as that obtained by Bai and Pollard (2000) and are discussed in more detail in the next section.

Secondly, FE model corresponding to the layered metal/ceramic microstructure described in Section 2 was created (Fig. 5). One quarter of the representative segment (Fig.2, left) was built in ABAQUS in order to investigate dependence of the stress field on the transverse coordinate  $x_3$  for different crack spacings (parameter  $S$ ). Boundary conditions reproducing tensile loading ( $\bar{\sigma}_{11} = \bar{\sigma}_{12} = 0$ ) were applied to the segment. Material behaviour of the metallic and ceramic layers was modelled as elastic, with Young's moduli, Poisson's ratio and layer thicknesses data given in Table 1. FE modeling allowed us to estimate numerically

the thickness of the shear layer for different crack spacings and use these results in the analytical modelling.

#### 4. RESULTS AND DISCUSSION

FE model presented in Fig. 4, which corresponds to numerical model of Bai and Pollard (2000), was used to verify FE model for the metal/ceramic composite. Results of the plane-strain calculations are plotted in Fig. 6 and show the distribution of the normal stress component in the direction perpendicular to the fractures ( $\sigma_{22}$ ) along the line OA (refer to Fig. 4) as a function of fracture spacing to layer thickness ratio ( $S/T_f$ ). The left side of the graph shows the stress values obtained by Bai and Pollard (2000) and the right side – present calculations using ABAQUS. In the present study, only the curves for  $S/T_f = 0.7, 1.0, 1.3$  were produced and very good correspondence with the results of Bai and Pollard (2000) was observed. Figure 6 shows also that when the fracture spacing reaches some critical value, the stress between cracks changes from tensile to compressive which can have decisive influence on the failure evolution.

After verification, numerical modelling of layered metal/ceramic microstructure presented in Fig. 5 was carried out. For large crack spacings, axial stress  $\sigma_{22}^{(c)}$  in the ceramic layer between the cracks away from crack surfaces was found to be tensile (Fig. 7a). As crack density increases and crack spacing becomes smaller, a region of compressive stress in the ceramic layer emerges (Fig. 7b, c). There is also a region of high tensile stresses in the ceramic layer in the vicinity of ceramic/metal interface, indicating possibility of debonding as competing failure mechanism.

Distribution of shear stress  $\sigma_{23}$  is shown in Fig. 8. For estimation of the shear layer thickness for different fracture spacing the distribution of the shear stress was studied along the nodes-path corresponding to the largest absolute values of the negative (Path 2) and positive (Path 1) shear stresses (see Fig. 8, left). Shear stress as a function of the  $x_3$  coordinate along the path is presented in Fig. 8, right, for the whole metallic layer with zooming in the shear layer as insert. The shear layer thickness was estimated as distance between the crack tip and the position along the  $x_3$  coordinate for which the shear stress is equal to zero. This procedure was carried out for different half-spacing to layer thickness ratios  $s/h_c = 0.7, 1.0, 1.3$  and corresponding ratios  $h_s/h_m = 0.17, 0.22, 0.27$  were obtained. For three studied half-spacing to layer thickness ratios  $s/h_c = 0.7, 1.0, 1.3$  the thickness of the shear layer increases with increasing of the distance between the cracks and the linear shape of the shear stress is only the first approximation to the numerical non-linear graph. Numerically estimated shear layer thicknesses were used as input in the analytical model.

Figure 9 shows distribution of the normalized axial stress  $\tilde{\sigma}_{22}^{(c)}/\bar{\sigma}_{22}$  under uniaxial tensile loading ( $\bar{\sigma}_{11} = \bar{\sigma}_{12} = 0$ ) as a function of distance  $x_2$  for a range of half-spacing to layer thickness ratios  $s/h_c$ . According to the analytical model, the average axial stress between the two existing cracks is tensile, with its value decreasing as the distance between two neighboring cracks becomes smaller.

Table 2 shows reduction of the composite's Young's modulus as predicted by the Equivalent Constraint Model and FE simulation for a range of relative crack densities  $D_c = h_c/s$ . The value of Young's modulus  $E_2$  for composite with cracks is normalised by its value  $\hat{E}_2$  in the undamaged state and given as a reduction ratio  $E_2/\hat{E}_2$ . The shear layer thickness was taken

as  $h_s = 0.15h_m$ . It can be seen that predictions based on the analytical model are in good agreement with FE model.

Reduction of all in-plane elastic properties of the composite as a function of relative crack density is shown in Fig. 10 for two ceramic contents: 35% and 45%. To facilitate the analysis, the values of stiffness properties for composite with cracks are normalised by their respective values for the undamaged composite and are plotted as reduction ratios  $E_1 / \hat{E}_1$ ,  $E_2 / \hat{E}_2$ ,  $G_{12} / \hat{G}_{12}$ ,  $\nu_{12} / \hat{\nu}_{12}$  and  $\nu_{21} / \hat{\nu}_{21}$  against the relative crack densities  $D_c = h_c / s$ . It can be seen that multiple cracking significantly reduces not only composite's Young's modulus  $E_2$  (i.e. modulus in the direction normal to the cracks), but also in-plane shear modulus  $G_{12}$  and Poisson's ratio  $\nu_{21}$ . For example, for the relative crack density of  $D_c = h_c / s = 0.25$ , which is roughly corresponds to what is observed in Fig.1, the reduction in Young's modulus  $E_2$  and Poisson's ratio  $\nu_{21}$  is approximately 40%. As expected, Young modulus  $E_1$  (i.e. modulus in the direction parallel to the cracks) is not affected by the presence of cracks. Poisson's ratio  $\nu_{12}$  increases slightly with increasing  $D_c$ , the reason being that Poisson's ratios  $\nu_{12}$  and  $\nu_{21}$  are not independent from each other, but related as  $\nu_{12} / E_1 = \nu_{21} / E_2$ .

Experimental data for metal/ceramic composites are required for comparison purposes, which are currently not available in the literature and this could become a task for future work. The non-linear behaviour of the shear stresses in the shear layer and also dependence of the shear layer thickness on the fracture spacing are also interesting subjects of future studies.

## 5. CONCLUSIONS

The cracked microstructure of single domain metal/ceramic composite sample is modeled by analytical and computational approaches. The results obtained by finite elements analysis are consistent with observations made by Bai and Pollard (2000). According to the obtained results, the average axial stress between the two cracks is decreasing with decreasing the distance between the cracks. Using FE modeling the shear layer thickness for different crack spacings is calculated and used as input in the analytical model. Stress field is determined used a modified 2-D shear lag approach and a finite element method. The Equivalent Constraint Model can be applied to predict degradation of stiffness properties of the sample due to multiple transverse cracking.

## REFERENCES

1. Clyne TW (2000) *Comprehensive Composite Materials*, vol. 3: Metal Matrix Composites. Oxford UK: Pergamon. 842 pp
2. Evans A, San Marchi C, Mortensen A (2003) *Metal Matrix Composites in Industry: An Introduction and a Survey*. Dordrecht: Kluwer. 423 pp.
3. Miracle DB (2005) Metal matrix composites – from science to technological significance. *Composites Science and Technology* 65: 2526-2540.
4. Chawla N, Chawla KK (2006) *Metal matrix composites*. New York, Springer.
5. Mortensen A, Llorca J (2010). *Metal Matrix Composites*. *Annual Review of Materials Research* 40: 243-270.
6. Fukasawa T, Ando M, Ohji T, Kanzaki S (2002) Synthesis of porous Silicon Nitride with unidirectionally aligned channels using freeze-drying process. *Journal of American Ceramic Society* 85: 2151-2155.
7. Mattern A, Hucher B, Staudenecker D, Oberacker R, Nagel A, Hoffmann M J (2004) Preparation of interpenetrating ceramic–metal composites. *Journal of European Ceramic Society* 24(12): 3399-3408.
8. Deville S, Saiz E, Nalla RK, Tomsia, AP (2006) Freezing as a path to build complex composites. *Science* 31: 515-518.
9. Roy S, Wanner A (2008) Metal/ceramic composites from freeze-cast ceramics preforms, Domain structure and elastic properties. *Composites Science and Technology* 68: 1136-1143.
10. Roy S, Butz B, Wanner A (2010) Damage evolution and domain-level anisotropy in metal ceramics composites exhibiting lamellar microstructures. *Acta Materialia* 58: 2300-2312.

11. Ziegler T, Neubrand A, Piat R (2010) Multiscale homogenization models for the elastic behaviour of metal/ceramic composites with lamellar domains. *Composites Science and Technology* 70( 4): 664-670.
12. Roy S, Gebert J-M, Stasiuk G, Piat R, Weidemann KA (2011) Complete determination of elastic moduli of interpenetrating metal/ceramic composites using ultrasonic techniques and micromechanical modelling. *Materials Science and Engineering A* 528: 8226-8235.
13. Sinchuk Y, Roy S, Gibmeier J, Piat R, Wanner A (2013) Numerical study of internal load transfer in metal/ceramic composites based on freeze-cast ceramic preforms and experimental validation. *Materials Science and Engineering A* 585: 10-16.
14. Launey ME, Munch E, Alsem DH, Saiz E, Tomsia AP, Ritchie RO (2010) A novel biomimetic approach to the design of high-performance ceramic metal-composites. *Journal of the Royal Society Interface* 7: 741-753.
15. Kashtalyan M, Soutis S (2011) Residual stiffness of cracked cross-ply composite laminates under multi-axial in-plane loading. *Applied Composite Materials* 18: 31-43.
16. Katerelos DTG, Kashtalyan M, Soutis C, Galiotis C (2008) Matrix cracking in polymeric composites laminates: Modelling and experiments. *Composites Science and Technology* 68: 2310-2317.
17. Huang Y, Zhang HW, Wu F (1994) Multiple cracking in metal-ceramic laminates. *International Journal of Solids and Structures* 20: 2753-2768.
18. Huang Y, Zhang HW (1996) The role of metal plasticity and interfacial strength in the cracking of metal/ceramic laminates. *Acta Metallurgica et Materialia* 43: 1523-1530.



19. Shaw MC, Clyne TW, Cocks ACF, Fleck NA, Pateras SK (1996) Cracking patterns in metal-ceramic laminates: Effects of plasticity. *Journal of the Mechanics and Physics of Solids* 44: 801-821
20. Hwu KL, Derby B (1999) Fracture of metal/ceramic laminates—I. Transition from single to multiple cracking. *Acta Materialia* 47: 529-543.
21. Hwu KL, B (1999) Fracture of metal/ceramic laminates—II. Crack growth resistance and toughness. *Acta Materialia* 47: 545–563.
22. Zhang, J. Fan, J. and Soutis, C. (1992) Analysis of multiple matrix cracking in  $[\pm\theta_m/90_n]_s$  composite laminates Part 1: In-plane stiffness properties. *Composites* 23(5), 291-298
23. Kashtalyan M, Soutis S (1999) A study of matrix crack tip delaminations and their influence on composite laminate stiffness. *Advanced Composites Letters* 8: 149-155.
24. Kashtalyan M, Soutis S (2006) Modelling off-axis ply matrix cracking in continuous fibre-reinforced polymer matrix composite laminates. *Journal of Materials Science* 41: 6789-6799.
25. Kashtalyan M, Soutis S (2013) Predicting residual stiffness of cracked composite laminates subjected to multi-axial inplane loading. *Journal of Composite Materials* 47: 2513-2524
26. Bai T, Pollard DD (2000) Fracture spacing in layered rocks: a new explanation based on the stress transition. *Journal of Structural Geology* 22: 43-57.
27. ABAQUS, Simulia, Providence, RI, USA, <http://www.3ds.com/products-services/simulia/>, Accessed 4 June 2015.

## TABLES

Table 1. Properties of the constituents

Constituent	Young's modulus (GPa)	Poisson's ratio	Layer thickness (mm)	Shear modulus (GPa)
Aluminium alloy Al-12Si	80	0.33	0.3	30
Alumina Al <sub>2</sub> O <sub>3</sub>	390	0.24	0.2	157.26

Table 2. Reduction ratio for the composite Young's modulus  $E_2 / \hat{E}_2$

Relative crack density $D = h_c / s$	Equivalent Constraint Model	FE simulation	Difference, %
0.1	0.7805	0.7889	-1.06
0.2	0.6461	0.6514	-0.819
0.5	0.4421	0.4358	1.45
0.8	0.3571	0.3486	2.44

## FIGURE CAPTIONS

**Figure 1** Transverse cracks in ceramic layer of metal/ceramic composite with lamellar microstructure

**Figure 2** Schematics showing a metal/ceramic composite sample with multiple tunnelling cracks in the ceramic layer (left) and a representative segment bounded by two cracks (right)

**Figure 3** Variation of the out-of-plane shear stress

**Figure 4** FE model reproducing experimentally validated numerical studies of Bai and Pollard (2000)

**Figure 5** FE model of a quarter of the representative segment with thicknesses  $2h_c$  and  $h_m$  of the ceramic and metallic layers.  $2s$  is the crack spacing

**Figure 6** Distribution of the normal stress component  $\sigma_{22}$  in the direction perpendicular to the fracture along the line OA (see Fig. 4) as a function of fracture spacing to layer thickness ratio ( $S/T_f$ ): on the left the part of the symmetric graph – results of Bai and Pollard (2000), on the right of the graph – results obtained in the present study

**Figure 7** Axial stress distribution for three crack half-spacing to layer thickness ratios: a)  $s/h_c = 1.3$ ; b)  $s/h_c = 1.0$ ; c)  $s/h_c = 0.7$

**Figure 8** Shear stress distribution (left) and shear stress distribution along Paths 1 and 2 (right) for three crack half-spacing to layer thickness ratios: a)  $s/h_c = 0.7$ ; b)  $s/h_c = 1.0$ ; c)  $s/h_c = 1.3$

**Figure 9** Normalized axial stress  $\tilde{\sigma}_{22}^{(c)} / \bar{\sigma}_{22}$  in the ceramic layer as a function of co-ordinate  $x_2$  for a range of crack spacing to layer thickness ratios as predicted by: a) analytical model and b) finite element model

**Figure 10** Normalised stiffness properties of a metal/ceramic composite sample as a function of crack density: a) ceramic content 35%; b) ceramic content 45%

FIGURES

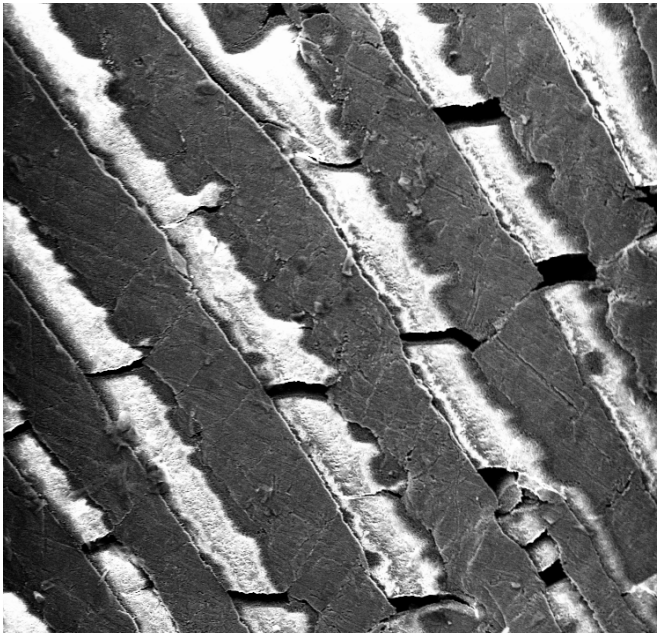


Figure 1.

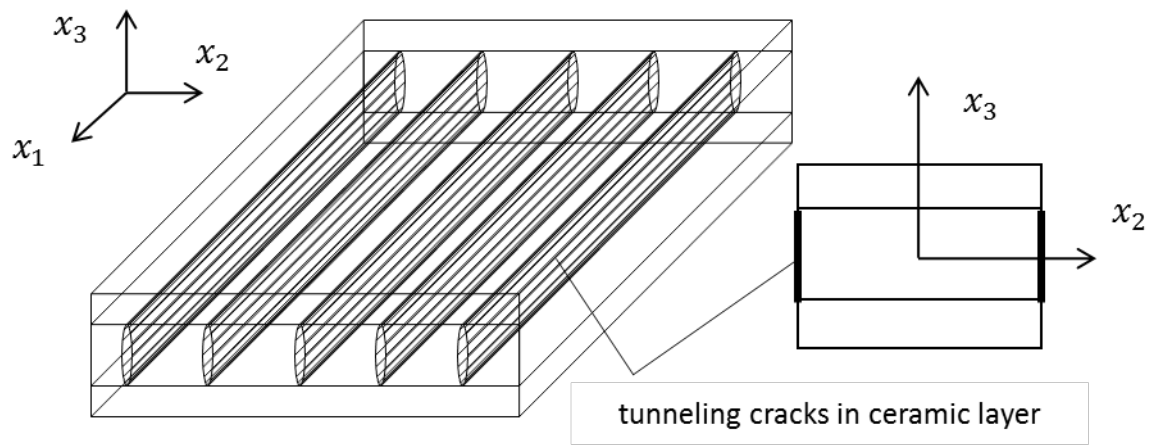


Figure 2.

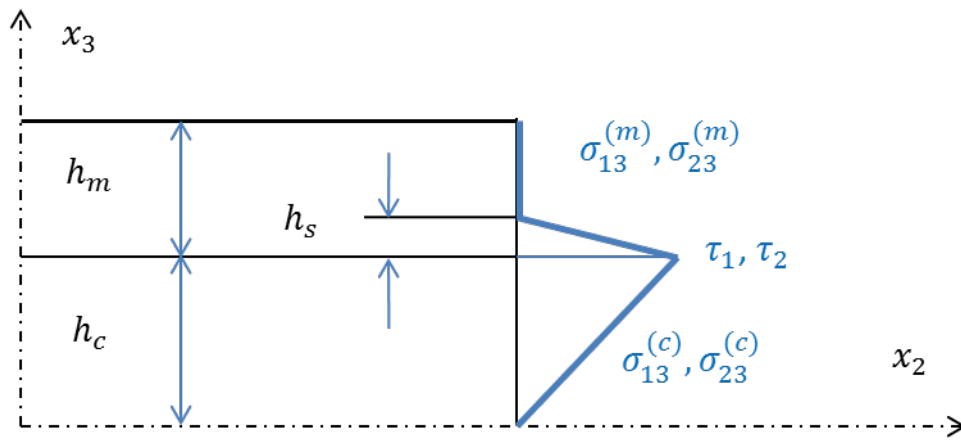


Figure 3.

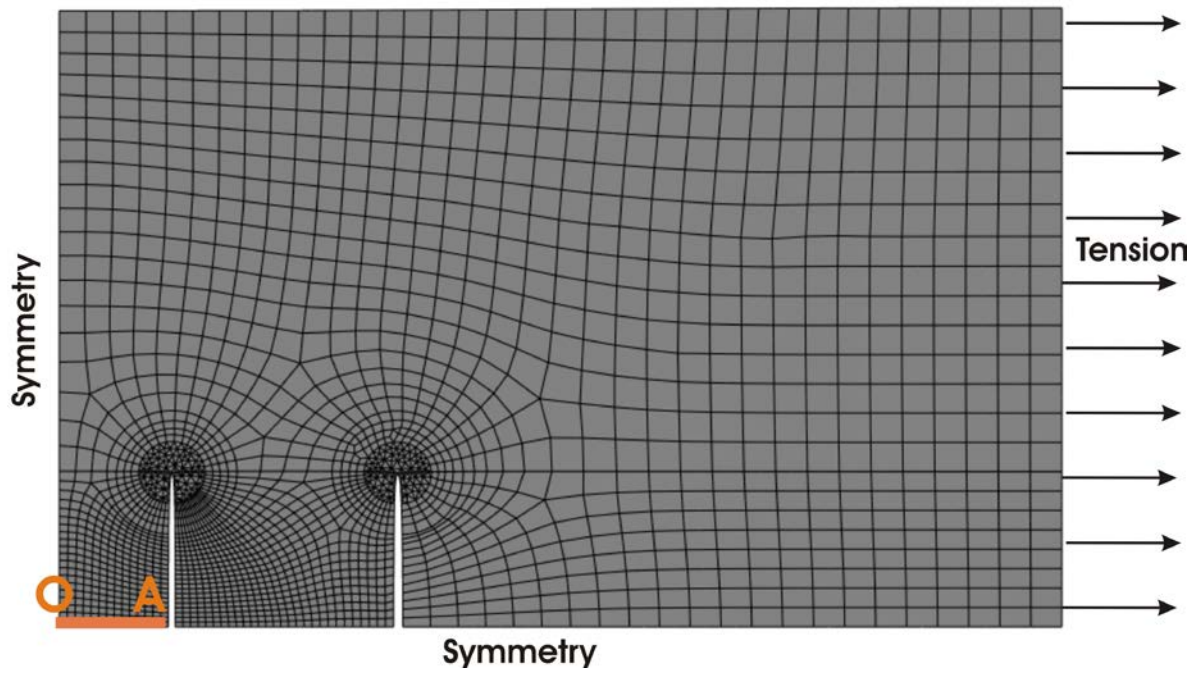


Figure 4.

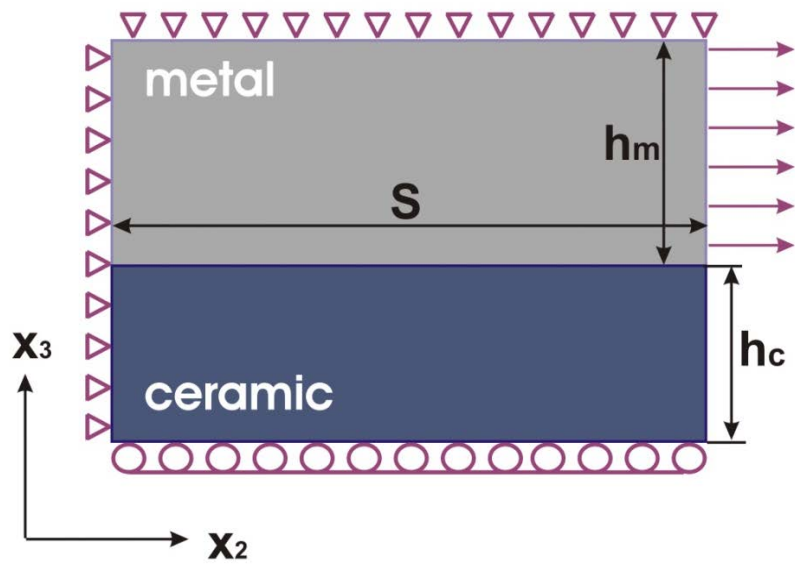


Figure 5.



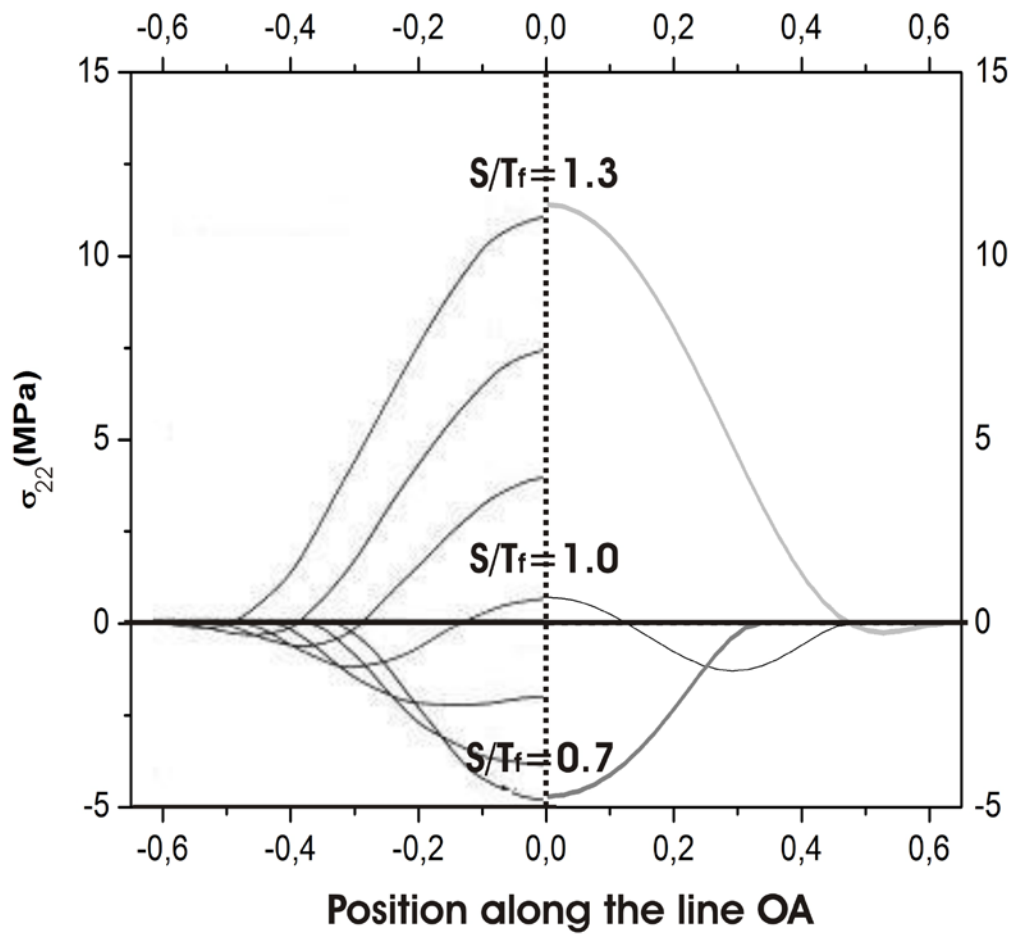
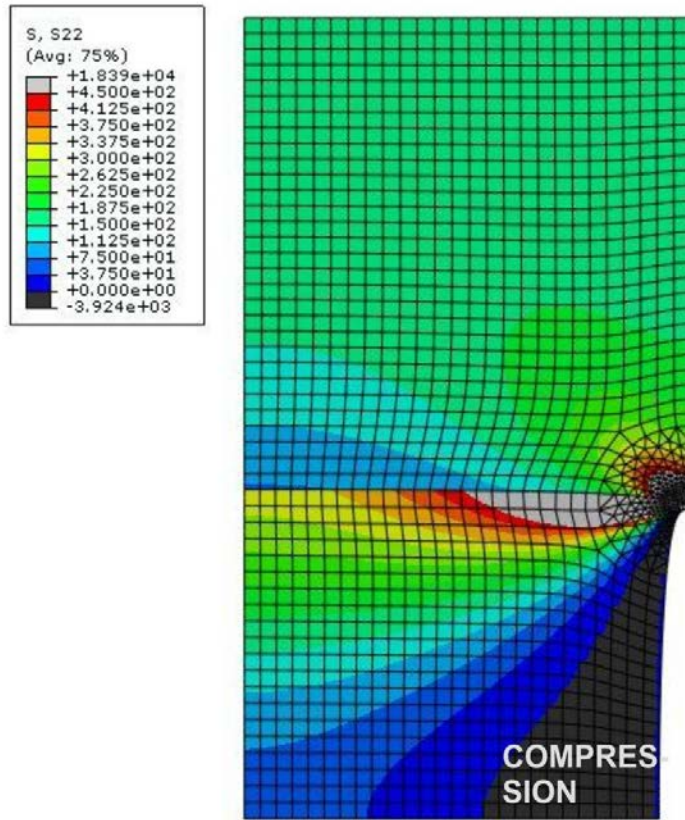
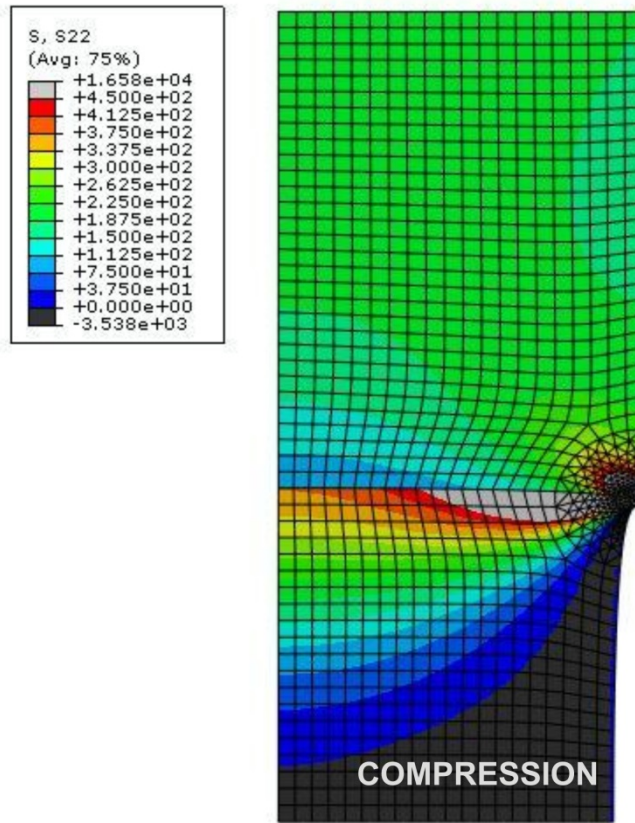


Figure 6.



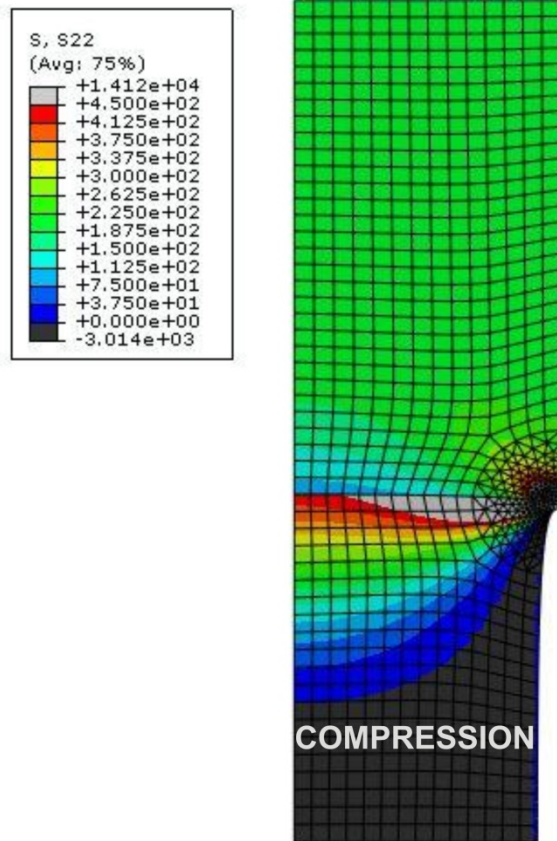
a)

Figure 7.



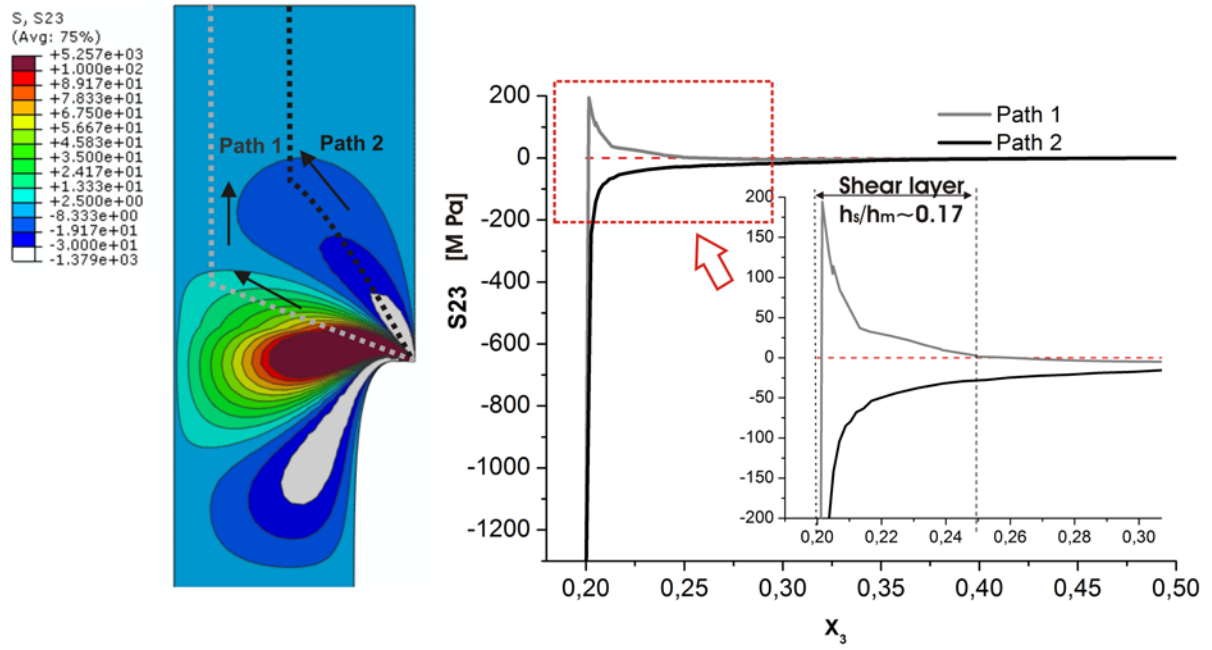
b)

Figure 7.



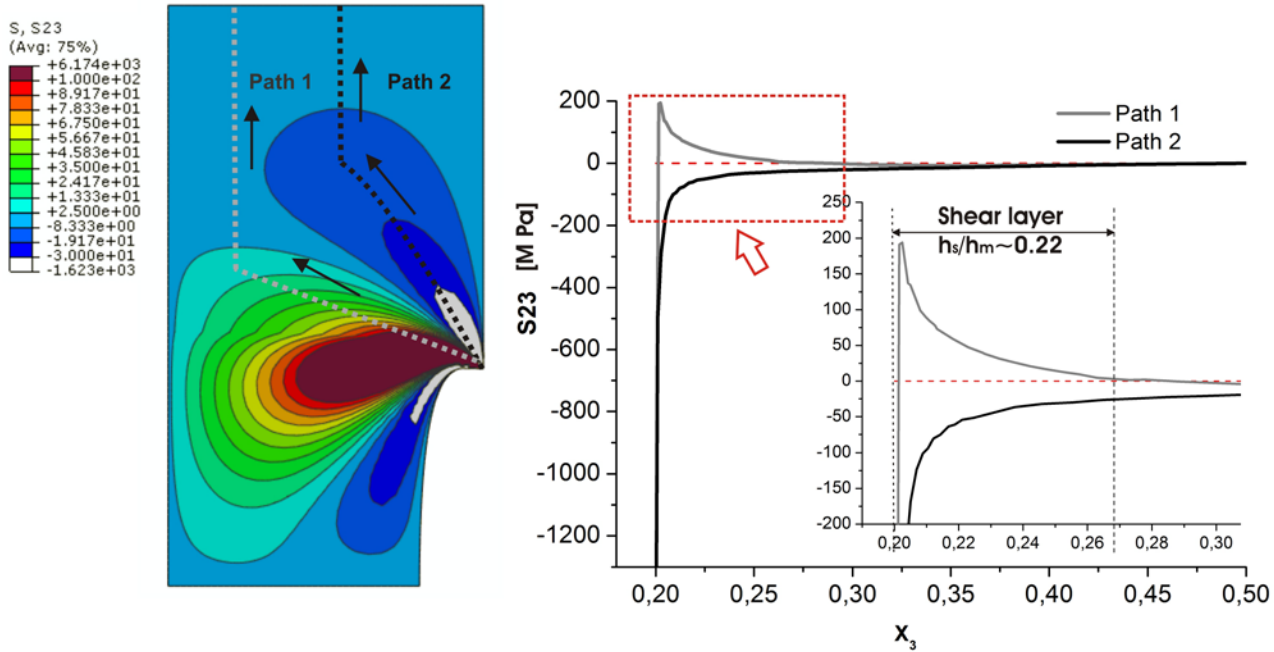
c)

Figure 7.



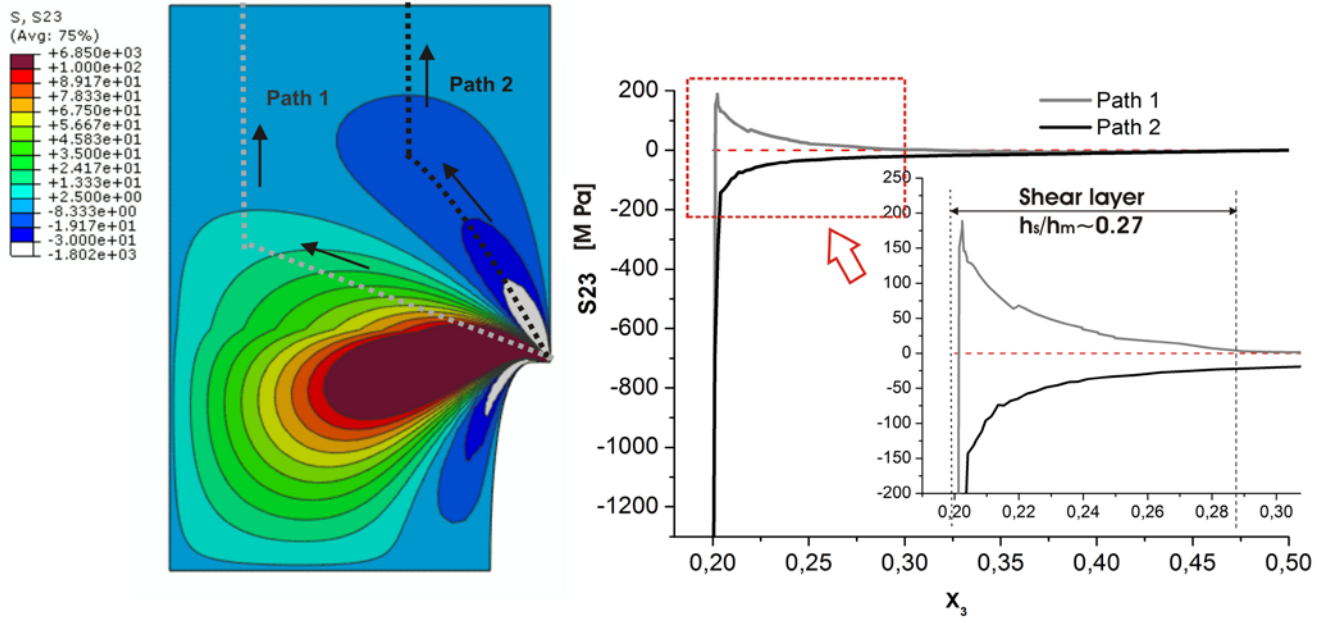
a)

Figure 8.



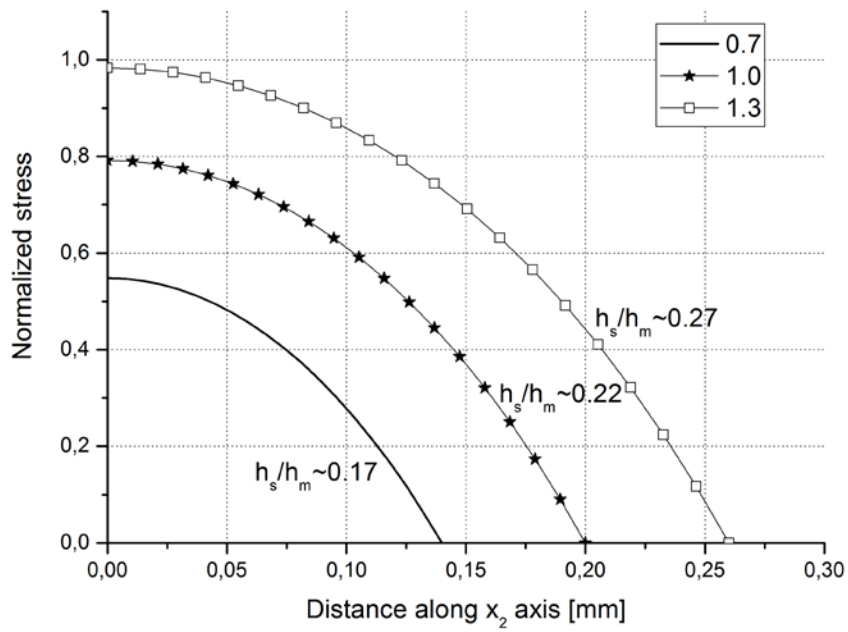
b)

Figure 8.

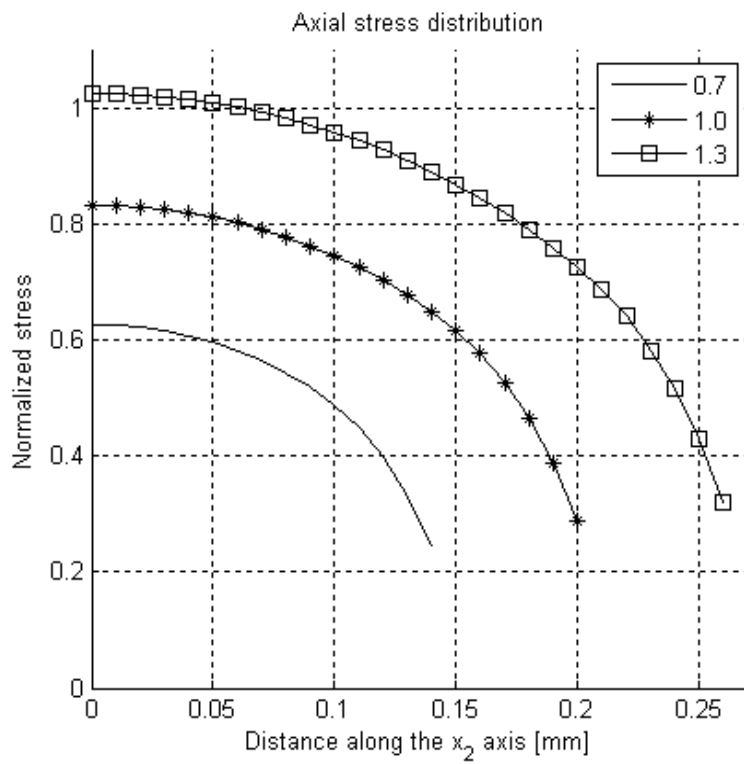


c)

Figure 8.



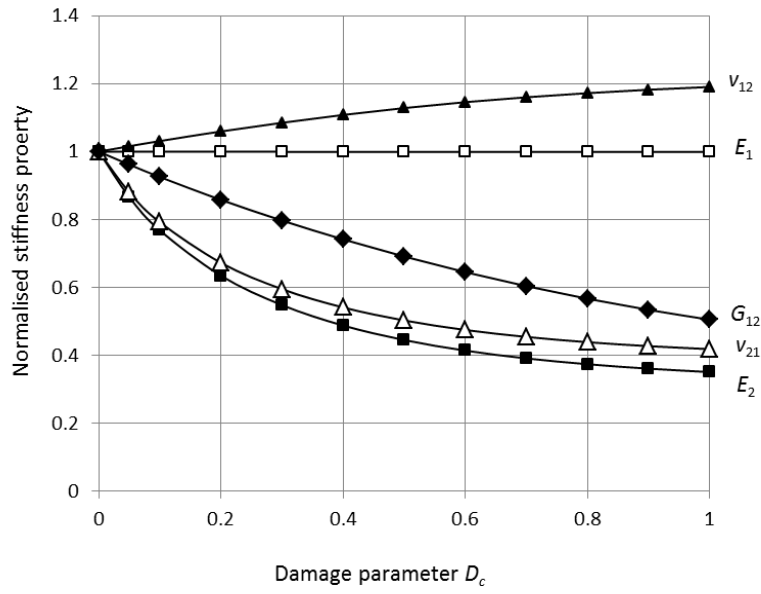
a)



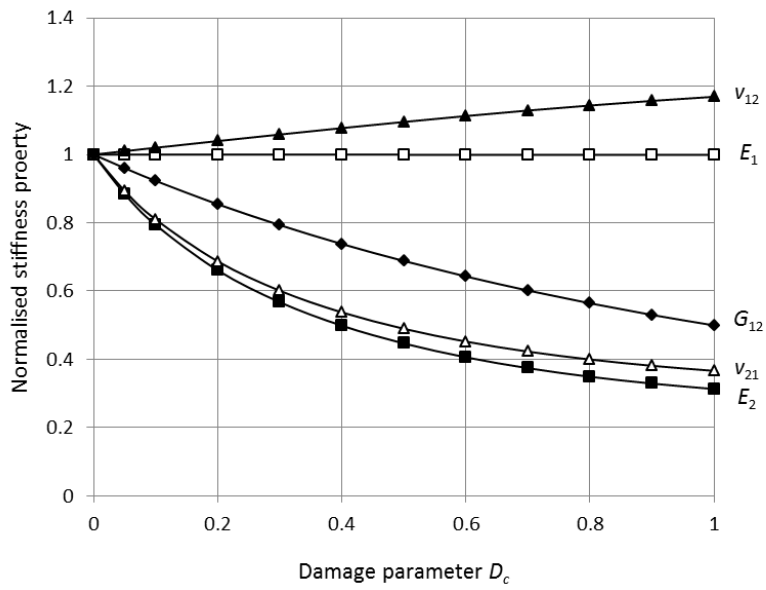
b)

Figure 9.





a)



b)

Figure 10.